

Effect of temperature on the photocatalytic properties of TiO₂-CeO₂ multilayer thin films obtained by spin coating method

(Efeito da temperatura nas propriedades fotocatalíticas de filmes finos multicamadas de TiO₂-CeO₂ obtidos por spin coating)

T. B. O. Nunes¹, N. F. Andrade Neto^{1*}, L. M. P. Garcia¹, R. M. Nascimento¹, M. R. D. Bomio¹, F. V. Motta¹

¹Federal University of Rio Grande do Norte, Department of Materials Engineering, Laboratory of Chemical Synthesis of Materials, P.O. Box 1524, Natal, RN, Brazil

Abstract

TiO₂-CeO₂ multilayer thin films were deposited by the spin coating method and calcined at 500 and 700 °C. Thin films were characterized by X-ray diffraction (XRD), field emission scanning electron microscopy (FE-SEM), atomic force microscopy (AFM), and diffuse reflectance spectroscopy. Photocatalytic properties were estimated by varying the concentration of the methylene blue dye (MB) when illuminated by UV radiation. The XRD patterns showed that the temperatures of 500 and 700 °C were effective to obtain TiO₂ and CeO₂ phases. The difference in the homogeneity of TiO₂ and CeO₂ films was evident in the AFM images, where the films showed an average roughness of 2.0 and 5.3 nm, respectively. The CeO₂-TiO₂ thin film obtained at 700 °C showed the best photocatalytic activity, reducing the concentration of MB by approximately 80%, while the CeO₂ and TiO₂ films obtained at 700 °C reduced only 20% and 29%, respectively. The reuse test showed that the thin films maintained their photocatalytic activity after 4 cycles, and there was no need for thermal treatment, indicating that it is an immobilized photocatalyst with high efficiency in the degradation of organic dyes.

Keywords: spin coating, multilayer thin films, CeO₂-TiO₂, photocatalytic reuse.

Resumo

Filmes finos multicamadas de TiO₂-CeO₂ foram depositados pelo método de spin coating e calcinados a 500 e 700 °C. Os filmes finos foram caracterizados por difração de raios-X (DRX), microscopia eletrônica de varredura por emissão de campo (MEV-FEG), microscopia de força atômica (MFA) e espectroscopia de reflectância difusa. As propriedades fotocatalíticas foram estimadas variando a concentração do corante azul de metileno (AM) quando iluminado por radiação UV. Os padrões de DRX mostraram que as temperaturas de 500 e 700 °C foram efetivas para obter as fases de TiO₂ e CeO₂. A diferença na homogeneidade dos filmes de TiO₂ e CeO₂ foi evidente nas imagens de MFA, onde os filmes apresentaram rugosidade média de 2,0 e 5,3 nm, respectivamente. Filme fino de TiO₂-CeO₂ obtido a 700 °C apresentou a melhor atividade fotocatalítica, reduzindo a concentração de AM em aproximadamente 80%, enquanto os filmes de CeO₂ e TiO₂ obtidos a 700 °C reduziram apenas 20% e 29%, respectivamente. O teste de reutilização mostrou que os filmes finos mantiveram sua atividade após 4 ciclos, não havendo necessidade de tratamento térmico, indicando ser um fotocatalisador imobilizado com alta eficiência na degradação do corante orgânico.

Palavras-chave: spin coating, filmes finos multicamadas, CeO₂-TiO₂, reuso fotocatalítico.


INTRODUCTION

The combination of different materials to optimize their properties has been extensively studied [1]. The interaction among different ions promotes synergy effects, generating properties not found by the isolated phases. These materials can be obtained as particulate materials (core-shell or composites) and thin films when deposited on alternating layers [2, 3]. The use of thin films stands out in comparison to particulate materials because they do not generate residues after being treated, and they are easy to be reused [4]. Thin

films can be obtained by various methods, such as atomic layer positioning [5], dip-coating [6], spin coating [7], and spray-pyrolysis [8].

The spin coating method is widely used because it is easy to use, has low-cost, and produces uniform films [9]. Due to these characteristics, the spin coating is used for the deposition of thin films of various materials in photocatalytic applications. Oxide materials, such as TiO₂ and CeO₂, are widely studied for photocatalysis because they have high chemical stability and the ability to degrade organic dyes [10, 11]. Besides, CeO₂ is also well studied for oxygen storage and mobility because of the easy conversion between the Ce³⁺ in Ce⁴⁺ oxidation states [12]. The synthesis of TiO₂ and CeO₂ multilayer films makes possible the

*netoandrade@ufrn.edu.br

 <https://orcid.org/0000-0003-1421-2904>

improvement of the properties of the isolated oxides, where CeO_2 acts to increase the chemical stability and reduce the rate of recombination of the charge carriers through the heterojunctions formed [13, 14]. Yi et al. [15] synthesized $\text{CeO}_2\text{-Bi}_2\text{MoO}_6$ heterostructures by hydrothermal method, obtaining superior optical properties than that obtained for the isolated materials. Cano-Franco et al. [16] showed that the $\text{TiO}_2\text{-CeO}_2$ combination shifts the absorption band to the visible region, reducing the energy required for the excitation of the electrons in the valence band to the conduction band.

In this study, TiO_2 and CeO_2 multilayer thin films were obtained by the spin coating method and calcined at 500 and 700 °C. The thin films were characterized by X-ray diffraction, field emission scanning electron microscopy, atomic force microscopy, and diffuse reflectance spectroscopy. The activity of TiO_2 and CeO_2 multilayer thin films was analyzed in comparison to the pure oxide films by the variation in the concentration of the methylene blue dye when illuminated by UV radiation. The photocatalytic reuse of the thin films was investigated by 4 consecutive cycles, drying the films in the air after each cycle.

MATERIALS AND METHODS

Cerium nitrate (Sigma Aldrich, 99%), titanium isopropoxide (Sigma Aldrich, 97%), citric acid (Synth, 99.5%), ethylene glycol (Synth, 99.5%), and deionized water were used to obtain the polymer resins by polymeric precursor method (PPM). For the PPM method, cerium nitrate was dissolved in water, and isopropoxide was dissolved in isopropyl alcohol; the solutions were kept under stirring at 60 °C. After full dissolution, citric acid was used to form the metal citrate. Finally, ethylene glycol was added, and the resin was stirred until the viscosity reached 25 cps. The resins were deposited on (100) silicon substrates. The cleaning of the substrates was divided into two steps. First, the substrates were washed with water and neutral soap; then, they were kept in an ultrasonic bath for 15 min in isopropyl alcohol and 15 min in deionized water. In the second step, the substrates were immersed in a solution of deionized water,

ammonium hydroxide, and hydrogen peroxide maintained at 70 °C for 15 min. Drying occurred at room temperature. The resins were deposited by the spin coating method, with a rotation speed of 7000 rpm for 20 s. Then, the resin was calcined at two temperatures, 500 and 700 °C, to obtain the thin film layer. The process was repeated to obtain a thin film composed of 4 layers. The multilayer films were obtained with the CeO_2 and TiO_2 in intercalated layers, varying the oxide that remained on the first layer. Fig. 1 illustrates the multilayer thin film-forming model.

Thin films were characterized by X-ray diffraction (XRD) at low angles with a diffractometer (Shimadzu, XRD-6000) using $\text{CuK}\alpha$ radiation (1.5418 Å). Field emission scanning electron microscopy (FE-SEM) was used to observe the surface and cross-section of the thin films. The film thickness was determined using ImageJ software [17]. Atomic force microscopy (AFM) was performed with a microscope (Shimadzu, SPM-9700) to obtain information about the surface roughness of thin films. UV-visible spectroscopy was performed with a spectrophotometer (Shimadzu, UV-2550) in the diffuse reflectance mode, with wavelength ranging from 200 to 900 nm. Kubelka-Munk [18] function was used to convert reflectance data in absorption, and Wood and Tauc equation [19] was applied based on the direct permissible transition ($k=1/2$). The linear portion of the curve was extrapolated to $y\text{-axis}=0$ to estimate the band gap (E_{gap}). The photocatalytic activity of the thin films was estimated by the variation of the concentration of the methylene blue dye (MB) by the test time when the samples were submitted to UV radiation. Thin films with 6x6 mm were placed in contact with 10 mL of 10^{-5} mol.L⁻¹ methylene blue dye ($\text{C}_{16}\text{H}_{18}\text{ClN}_3\text{S}$, Mallinckrodt, 99.5% purity). At 30 min intervals, an aliquot was withdrawn to analyze the variation of the dye absorption band. After the first test, the film was washed and dried in the air; after drying, it was again placed in contact with the MB to carry out the subsequent cycle. This reuse process was repeated 3 times, resulting in 4 test cycles.

RESULTS AND DISCUSSION

Fig. 2 shows the XRD patterns obtained for the multilayer thin films. The CeO_2 characteristic peaks were characterized by the ICSD 88759 file of the cerianite phase (cubic system and spatial group Fm-3m). The characteristic peaks of TiO_2 were characterized by the ICSD 24276 file of the anatase phase (tetragonal system and spatial group I41/amd). In Fig. 2, it can be seen that the temperatures of 500 and 700 °C were effective in obtaining CeO_2 and TiO_2 thin films without the formation of secondary phases. The Scherrer equation [20], which relates the width of an XRD peak (full width at half maximum - FWHM) to the crystallite size, was used to investigate the effect of temperature on the peak width. For this, the most intense peak of each phase was used, which was (101) and (111) for TiO_2 and CeO_2 , respectively. Table I presents the crystallite size values obtained by the Scherrer equation. The energy provided by the increase in the

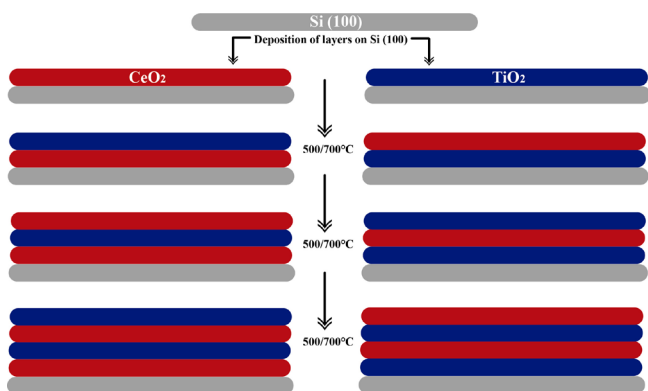


Figure 1: Scheme for the formation of $\text{TiO}_2\text{-CeO}_2$ multilayer thin films.

[Figura 1: Esquema para a formação dos filmes finos multicamadas de $\text{TiO}_2\text{-CeO}_2$.]

calcination temperature favored the growth of crystallites, as observed by the increase in the sharpness and intensity of the diffraction peaks [18]. Higher energy in the system, due to the calcination temperature, caused the particles to increase in size to reduce the total energy related to the particle's surface area [21]. A similar result was shown in another study [22], in which a higher annealing temperature generated thin films with larger crystallite size and crystallinity. According to Table I, the reduction in the microstrain of the unit cells was observed as the calcination temperature increased, due to the relaxation promoted by the higher energy supplied to the system.

Fig. 3 shows the micrographs obtained by FE-SEM for multilayer thin films calcined at 500 and 700 °C. It was noticed that when the upper layer was formed by TiO₂, the films presented a regular morphology and low porosity. The films had a higher porosity when CeO₂ was used as the top layer. It was also verified that as TiO₂ had a smaller particle size than CeO₂, it generated denser films. The thickness values in Table I were consistent with the results of the XRD patterns, where the increase in temperature generated larger grains, which consequently generated thicker films. Singh *et al.* [23] obtained thin films of TiO₂ by sputtering and calcination at 600 °C and observed that the thicker films provided higher densification due to their smaller average grain size, a fact opposite to that observed in this study, in which the thicker

films had larger grains. EDX analysis (energy-dispersive spectroscopy coupled to SEM) was performed in the TiO₂-CeO₂ and CeO₂-TiO₂ thin films calcined at 700 °C and the results are shown in Fig. 4. According to the chemical dot mapping, the TiO₂-CeO₂ film presented more CeO₂ at the surface. The opposite holds for the CeO₂-TiO₂ film, which presented more TiO₂ near the surface.

AFM was performed to obtain more information about the surface of the thin films. Fig. 5 shows the 3D micrographs obtained by AFM for TiO₂-CeO₂ (Figs. 5a and 5b) and CeO₂-TiO₂ (Figs. 5c and 5d) multilayer thin films obtained at 500 and 700 °C. As can be seen, an increase in the temperature provided the growth of grains on the film surface. The growth of grains changed the roughness of the films. According to the roughness values presented in Table I, it was observed that the CeO₂ thin films exhibited greater roughness than that of TiO₂, as well as when CeO₂ was in the upper layer. It is expected that the films formed by smaller grains have lower surface roughness [24].

The band gap (E_{gap}) of the materials is associated with the energy barrier found by the electrons when migrating from the valence band to the conduction band [25]. This value depends on several factors, such as intermediate energy levels between the bands and defects [26]. Wood and Tauc methodology [19] was used to estimate E_{gap} for the thin films obtained. Fig. 6 shows the absorbance curves by

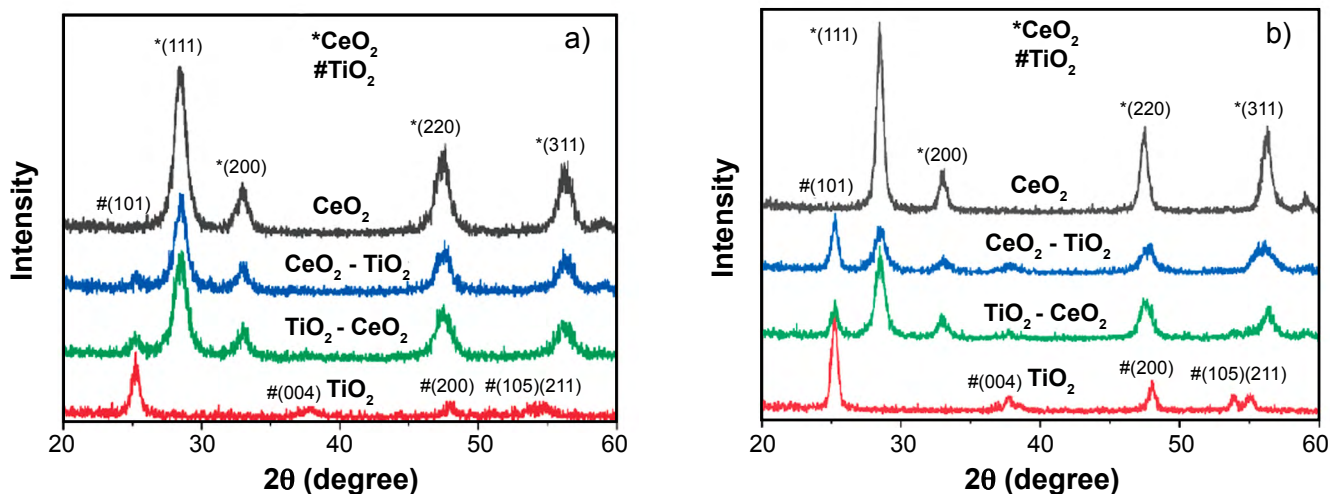


Figure 2: XRD patterns of the thin films obtained at 500 °C (a) and 700 °C (b).

[Figura 2: Difratoogramas de raios X dos filmes finos obtidos a 500 °C (a) e 700 °C (b).]

Table I - Crystallite size, thickness, and apparent roughness of the thin films obtained at 500 and 700 °C.

[Tabela I - Tamanho de cristalito, espessura e rugosidade aparente dos filmes finos obtidos em 500 e 700 °C.]

Sample	Crystallite size (nm)		Microstrain ($\times 10^{-3}$)		Thickness (nm)		Roughness (nm)	
	500 °C	700 °C	500 °C	700 °C	500 °C	700 °C	500 °C	700 °C
CeO ₂	7.7	13.5	1.11	0.63	232.1	239.7	5.26	7.96
CeO ₂ -TiO ₂	8.0	14.8	1.07	0.53	177.8	241.6	3.17	4.89
TiO ₂ -CeO ₂	8.8	14.5	1.01	0.57	193.7	241.0	3.83	6.47
TiO ₂	10.9	15.2	0.86	0.41	194.2	240.3	2.01	4.75

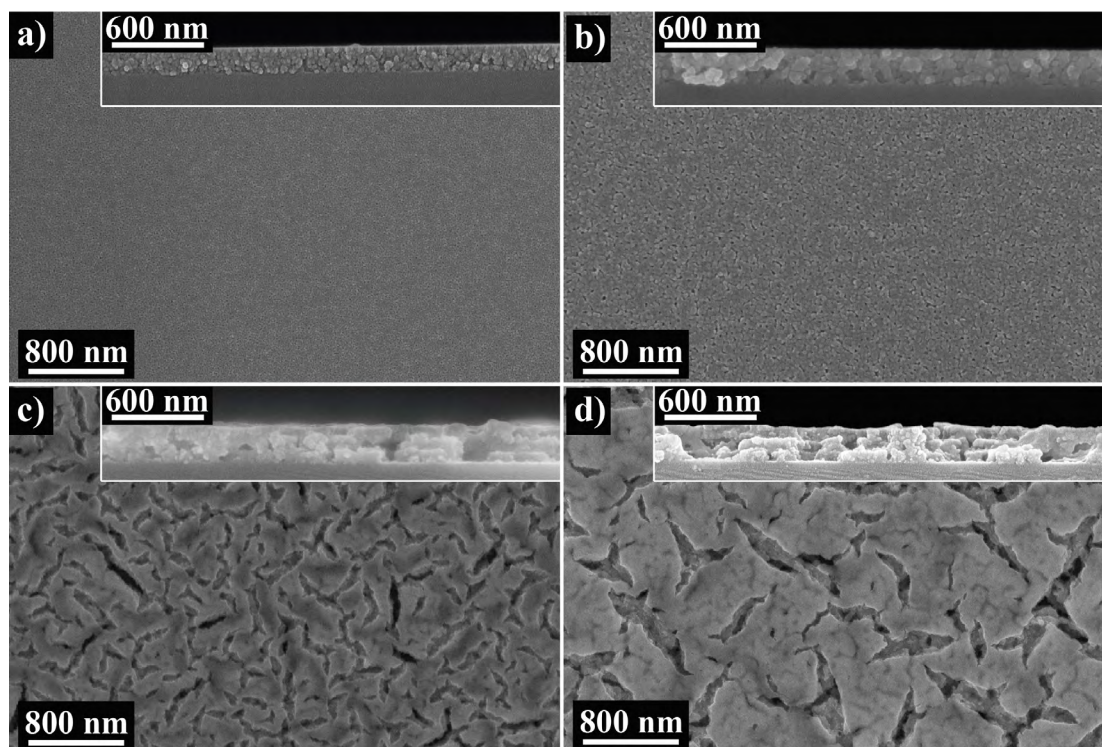


Figure 3: FE-SEM images of the surface and cross-section of the multilayer thin films of $\text{CeO}_2\text{-TiO}_2$ (a,b) and $\text{TiO}_2\text{-CeO}_2$ (c,d) obtained at 500 °C (a,c) and 700 °C (b,d).

[Figura 3: Imagens de MEV-FEG da superfície e da seção transversal dos filmes finos multicamadas de $\text{CeO}_2\text{-TiO}_2$ (a,b) e $\text{TiO}_2\text{-CeO}_2$ (c,d) obtidos em 500 °C (a,c) e 700 °C (b,d).]

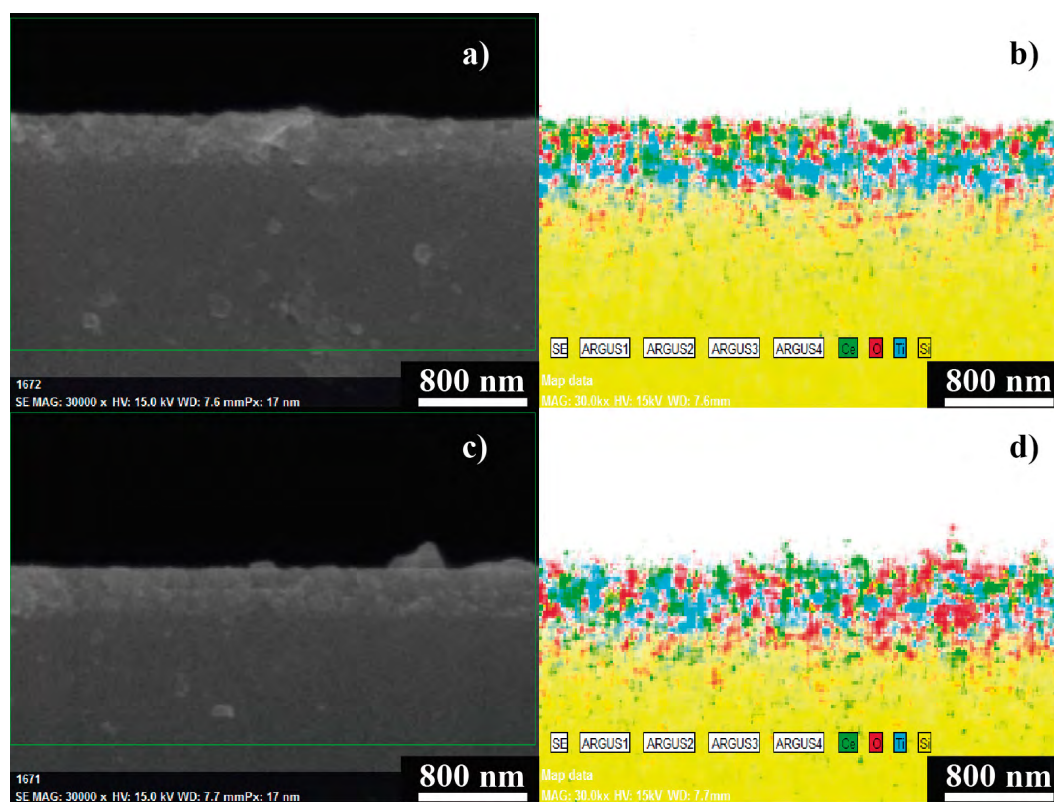


Figure 4: FE-SEM images of the cross-section (a,c) and respective EDX dot maps (b,d) for $\text{TiO}_2\text{-CeO}_2$ (a,b) and $\text{CeO}_2\text{-TiO}_2$ (c,d) thin films obtained at 700 °C.

[Figura 4: Imagens de MEV-FEG da seção transversal (a,c) e respectivo mapeamento elementar por EDX (b,d) para os filmes finos de $\text{TiO}_2\text{-CeO}_2$ (a,b) e $\text{CeO}_2\text{-TiO}_2$ (c,d) obtidos em 700 °C.]

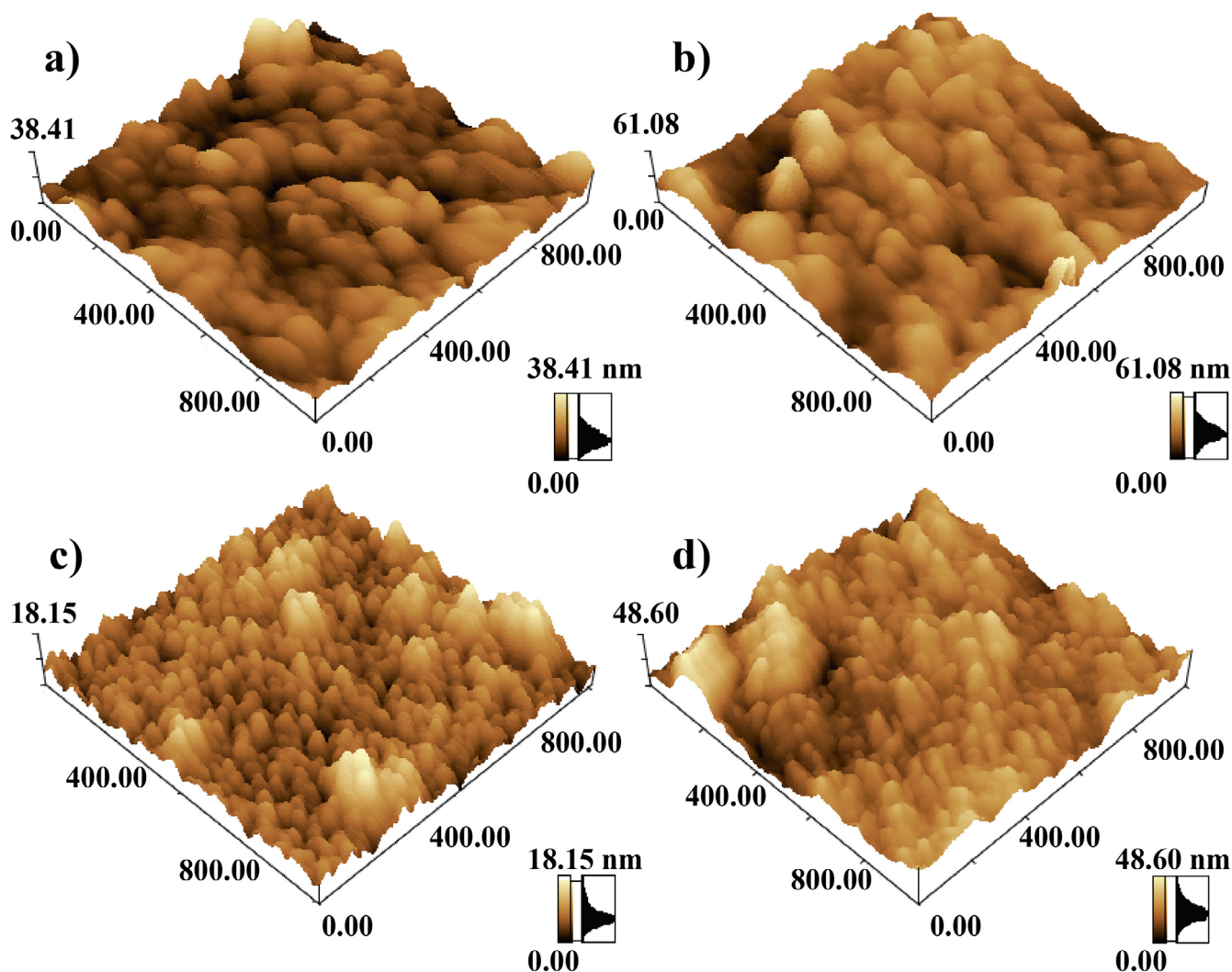


Figure 5: 3D micrographs obtained by atomic force microscopy for $\text{TiO}_2\text{-CeO}_2$ (a,b) and $\text{CeO}_2\text{-TiO}_2$ (c,d) thin films obtained at 500 °C (a,c) and 700 °C (b,d).

[Figura 5: Micrografias 3D obtidas por microscopia de força atômica para os filmes finos de $\text{TiO}_2\text{-CeO}_2$ (a,b) e $\text{CeO}_2\text{-TiO}_2$ (c,d) obtidos em 500 °C (a,c) e 700 °C (b,d).]

photon energy for the multilayer films. Thin films reduced their E_{gap} with increasing crystallization temperature. TiO_2 reduced E_{gap} from 3.00 to 2.77 eV, while CeO_2 reduced from 3.13 to 2.99 eV. The E_{gap} is generally associated with the size of particles, where smaller particles have a larger E_{gap} [27]. According to Fig. 6, the multilayer films did not show significant variation with the order of the layers. The E_{gap} of the multilayer films ranged between 2.90 and 2.98 eV and did not change with the temperature increase. The E_{gap} values obtained for the thin films were in agreement with the literature [28-31].

The photocatalytic activity of the thin films was estimated by the variation of the methylene blue dye (MB) concentration when submitted to UV-vis radiation. Fig. 7 shows the variation of MB concentration by the test time. Before the photocatalytic test, the thin films remained in contact with the dye for 60 min to eliminate possible adsorption effects. Fig. 7a shows the curves for the TiO_2

and CeO_2 thin films obtained at 500 and 700 °C and Fig. 7b shows the curves for multilayer thin films. It was seen that the increase in the crystallization temperature of the thin films from 500 to 700 °C increased the photocatalytic activity (Fig. 7a). For the thin film of TiO_2 calcined at 500 °C, MB concentration after 150 min reduced approximately 4%, while for the film obtained at 700 °C the reduction was approximately 29%. For CeO_2 thin film obtained at 500 °C, the reduction was about 17% of the MB concentration after 150 min, while for the CeO_2 thin film obtained at 700 °C the reduction was approximately 20%. Analyzing the increase in the photocatalytic activity of the films with the increase in calcination temperature, there was a more significant increase for the TiO_2 thin films. The photocatalytic process may be described by a first-order kinetic model with relation to the absorbance of the methylene blue [32], and the results obtained are shown in Figs. 7c and 7d. The graphs showed a linear relationship of $\ln(C/C_0)$ by the irradiation time and Eq.

A was used to determine the kinetic constant (k):

$$\frac{-\ln C_t}{C_o} = k.t \quad (\text{A})$$

where C_t is the absorbance of methylene blue at time t , C_o the initial absorbance, and t the irradiation time. According to Fig. 7, the kinetic constant (k) increased with increasing calcination temperature, where this increase was more evident for the multilayer films compared to the pure films. The increase in the photocatalytic activity of thin films is directly related to the increase in their surface area [5]. As shown in Table I, the increase in crystallization temperature increased the average surface roughness of the thin films, thus contributing to the increase of their contact area with the MB molecules. The higher photocatalytic activity of the TiO_2 film obtained at 700°C was in accordance with studies found in the literature, where TiO_2 thin films exhibit better photocatalytic activity than CeO_2 thin films [33-35]. Moreover, as previously seen, the increase of the calcination temperature promoted the relaxation in the TiO_2 and

CeO_2 unit cells, promoting a greater generation of oxygen vacancies [36]. Oxygen vacancies, in contact with the MB solution, generate reactive oxygen species (ROS), which have a high oxidative capacity, accelerating decolorization. The increase of the crystallization temperature also favored the photocatalytic activity of the multilayer thin films, as shown in Fig. 7b. CeO_2 - TiO_2 and TiO_2 - CeO_2 thin films obtained at 700°C showed high photocatalytic activity after 150 min, where the CeO_2 - TiO_2 thin films reduced approximately 80% of the MB concentration and the TiO_2 - CeO_2 thin films reduced 65%. CeO_2 - TiO_2 multilayers have higher photocatalytic activity and chemical stability for the degradation of organic dyes because the heterojunction formed between the CeO_2 and TiO_2 layers has a higher light absorption range than the single-phase compounds, causing the light to suffer multiple reflections and expand its propagation path, increasing the use of incident light [10, 14]. Obtaining CeO_2 and TiO_2 heterostructures provides the optimization of the properties of the isolated oxides, with higher photocurrent and photoelectric conversion [37]. The

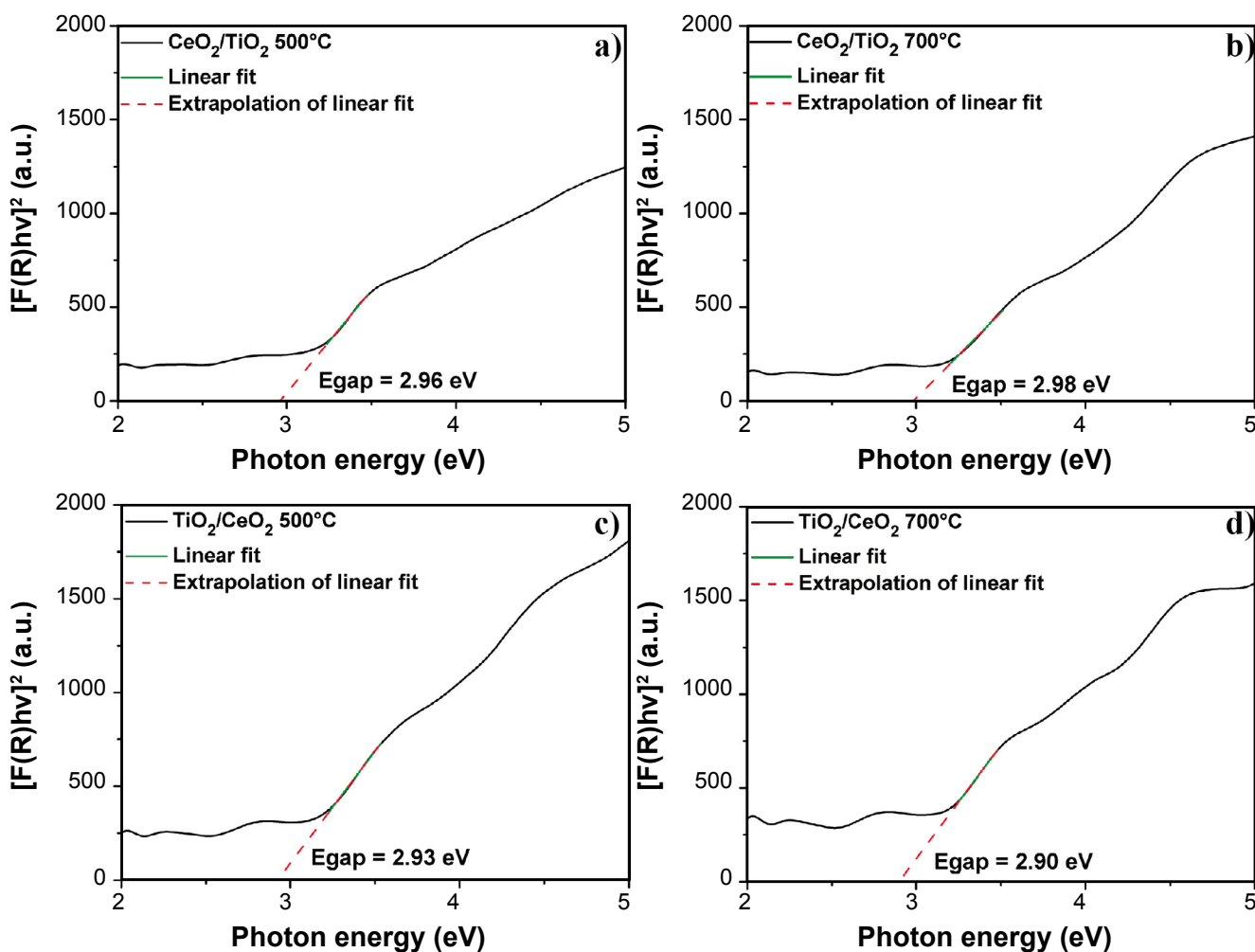


Figure 6: Wood and Tauc plots of CeO_2 - TiO_2 (a,b) and TiO_2 - CeO_2 (c,d) thin films obtained at 500°C (a,c) and 700°C (b,d), showing the extrapolation of the linear portion of the curve to estimate E_{gap} .

[Figura 6: Gráficos de Wood e Tauc dos filmes finos multicamadas de CeO_2 - TiO_2 (a,b) e TiO_2 - CeO_2 (c,d) obtidos em 500°C (a,c) e 700°C (b,d), mostrando extrapolação da porção linear da curva para determinação de E_{gap} .]

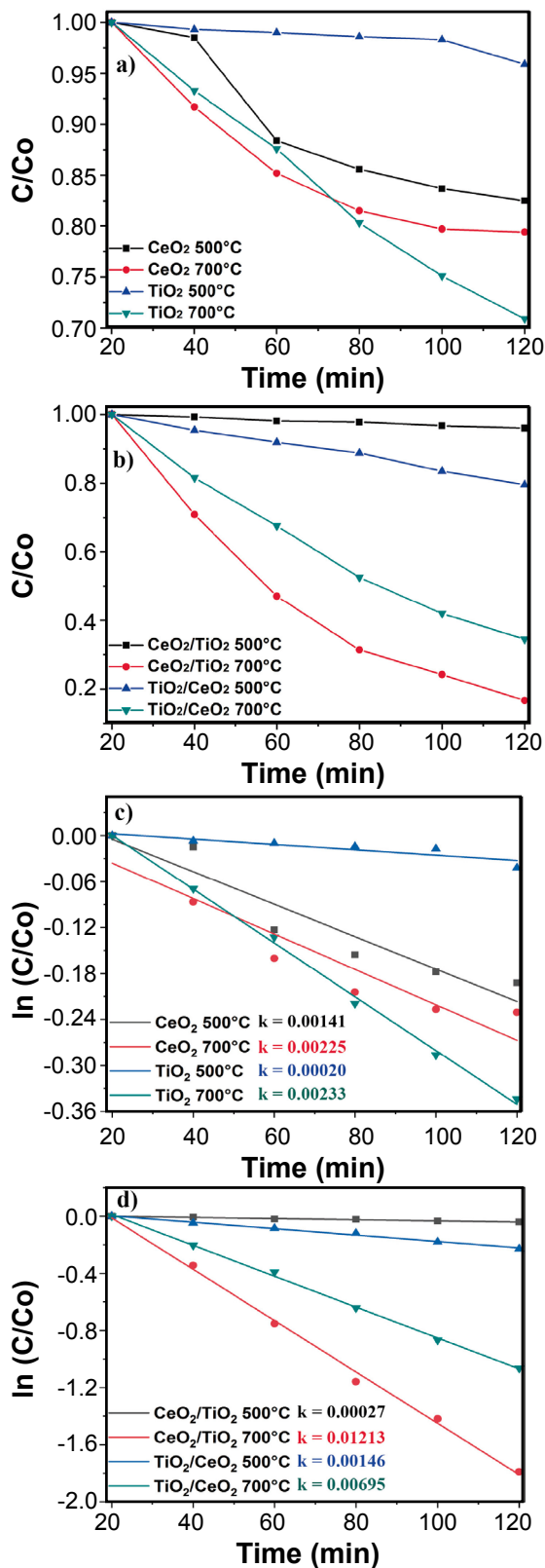


Figure 7: Variation of methylene blue concentration C/C_0 (a,b) and respective linearized plot $\ln(C/C_0)$ (c,d) with test time for pure (a,c) and multilayer (b,d) thin films obtained by spin coating.

[Figura 7: Variação da concentração de azul de metileno C/C_0 (a,b) e respectivo gráfico linearizado $\ln(C/C_0)$ (c,d) com o tempo de ensaio para os filmes finos puro (a,c) e multicamadas (b,d) obtidos por spin coating.]

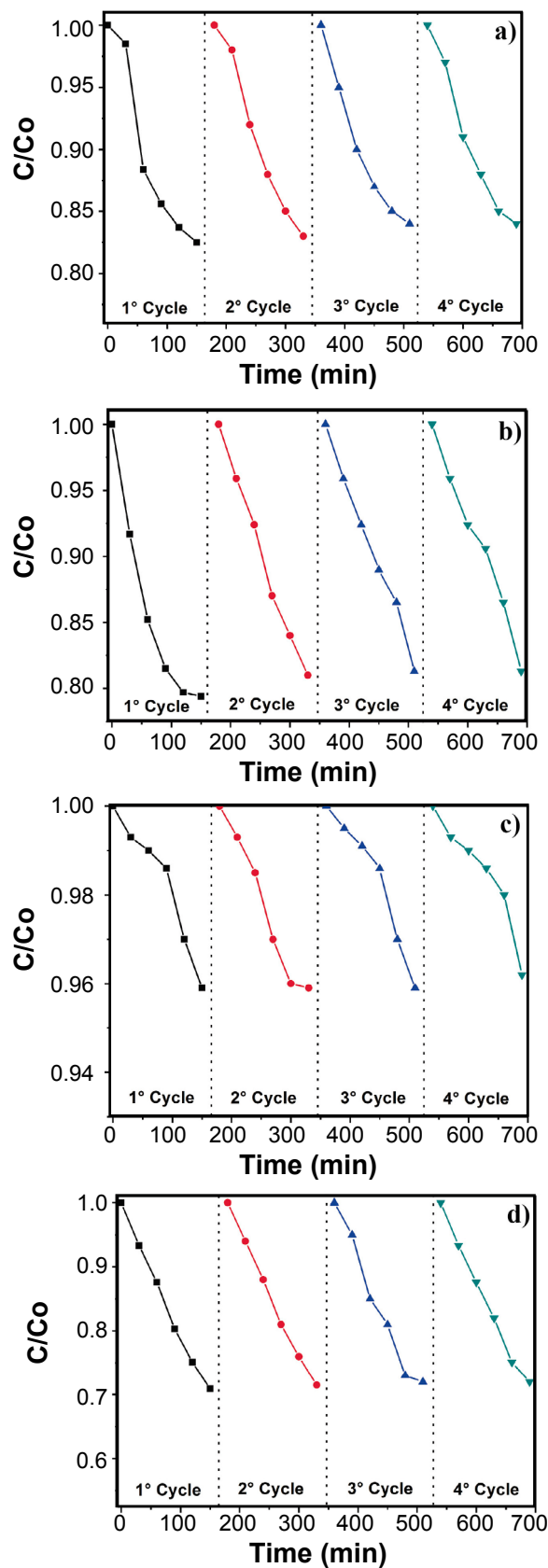


Figure 8: Results of photocatalytic reuse test (4 cycles) for thin films of CeO_2 (a,b) and TiO_2 (c,d) obtained at 500 °C (a,c) and 700 °C (b,d). [Figura 8: Resultados do ensaio de reuso fotocatalítico (4 ciclos) para filmes finos de CeO_2 (a,b) e TiO_2 (c,d) obtidos em 500 °C (a,c) e 700 °C (b,d).]

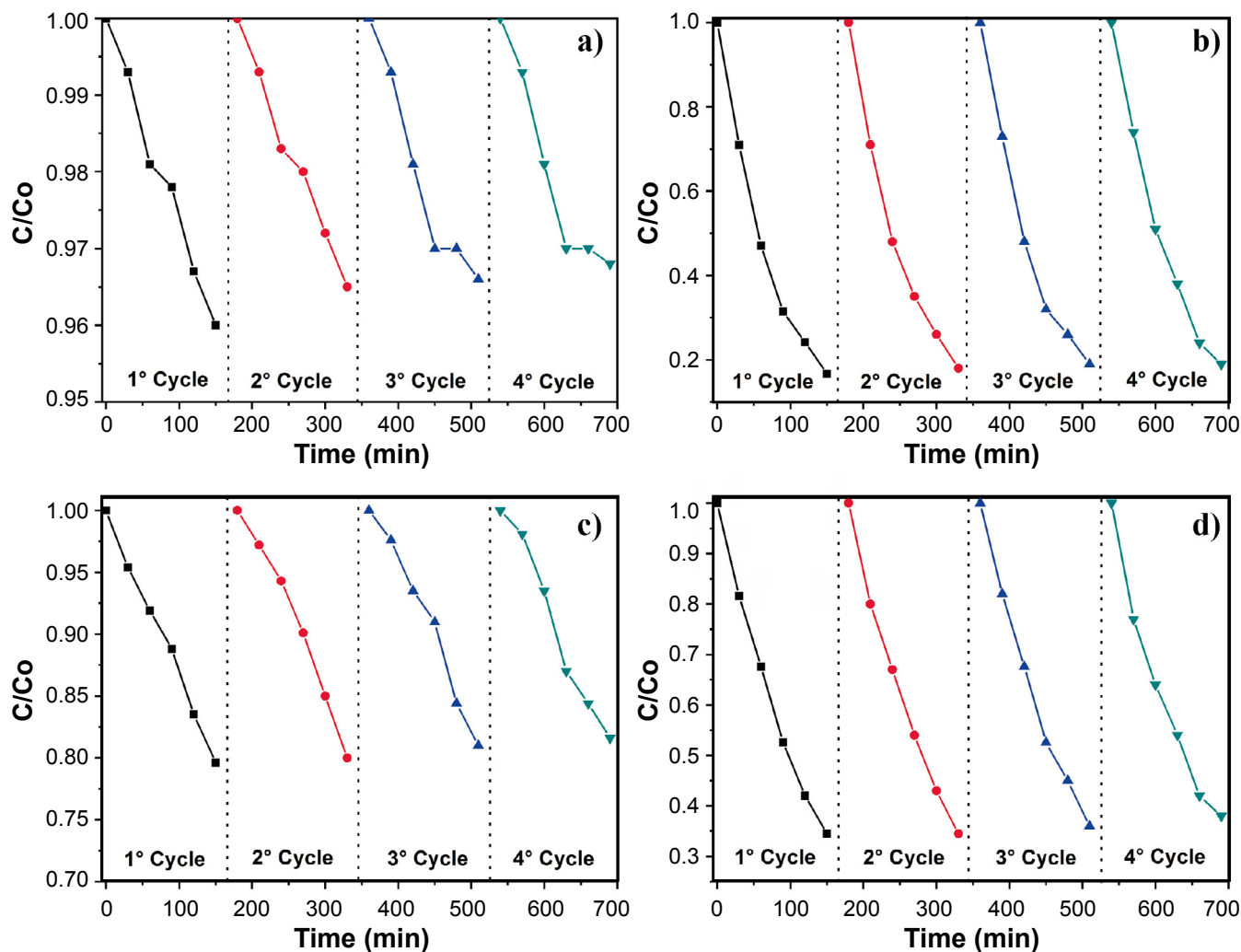


Figure 9: Results of photocatalytic reuse test (4 cycles) for thin films of CeO_2-TiO_2 (a,b) and TiO_2-CeO_2 (c,d) obtained at 500 °C (a,c) and 700 °C (b,d).

[Figura 9: Resultados do ensaio de reuso fotocatalítico (4 ciclos) para filmes finos de CeO_2-TiO_2 (a,b) e TiO_2-CeO_2 (c,d) obtidos em 500 °C (a,c) e 700 °C (b,d).]

photocatalytic results of multilayer films were consistent with those obtained with pure films, where the presence of TiO_2 on the surface promoted better catalytic performance.

The use of thin films as photocatalysts is widely studied due to the non-generation of secondary residues, which would require further treatment, as in the case of materials in powder form [38]. In addition to the high photocatalytic property, the film's ability to be reused is of great importance. The reusability of thin films takes into account their chemical stability and the maintenance of the photocatalytic property with the sequence of cycles to which they are submitted [7]. The reuse capacity of produced thin films in the photocatalytic activity was investigated through the use in 4 cycles, without accomplishing the heat treatment. Figs. 8 and 9 show the reuse curves for single and multilayer thin films. According to the curves shown in Fig. 8, it is observed that the photocatalytic activity of single-phase thin films was maintained, even after the 4 cycles tested. This fact was also observed for multilayer thin films, as shown in Fig. 9. The

maintenance of the photocatalytic property after the 4 cycles indicated that the thin films were chemically stable under UV radiation [39].

CONCLUSIONS

The spin coating method proved to be efficient for the deposition of uniform thin films, where TiO_2 film had higher densification than CeO_2 film due to the smaller particle size. Calcination temperatures of 500 and 700 °C were sufficient to obtain pure (TiO_2 or CeO_2) and multilayer (CeO_2-TiO_2 and TiO_2-CeO_2) films without forming secondary phases. Increasing the crystallization temperature caused the growth of crystallite size and film thickness; moreover, it increased the average apparent roughness of the films. The increase in the roughness and porosity of the thin films provided a higher surface area for contact with the dye, providing greater photocatalytic activity. The synergistic effect caused the multilayer films to have superior photocatalytic properties

than the single-phase films, where the multilayer film with the upper layer of TiO₂ reduced approximately 80% of the methylene blue concentration after 150 min of UV radiation; this film is a good candidate to be used in the treatment of textile effluents.

ACKNOWLEDGMENTS

This study was financed in part by the Coordenação de Aperfeiçoamento de Pessoal de Nível Superior - Brasil (CAPES) - Finance Code 001 and the authors give thanks for the financial support of the Brazilian research funding institutions: CNPq No. 307546/2014-4 and CAPES/PROCAD 2013/2998/2014.

REFERENCES

- [1] X. Hou, X. Wang, W. Mi, J. Alloys Compd. **765** (2018) 1127.
- [2] H. Miyazaki, T. Matsuura, T. Ota, Compos. Commun. **10** (2018) 136.
- [3] L.-Y. Lin, H.-Y. Lin, W.-L. Hong, L.-Y. Lin, Thin Solid Films **7** (2018) 69.
- [4] O.K. Echendu, S.Z. Werta, F.B. Dejene, V. Craciun, J. Alloys Compd. **769** (2018) 201.
- [5] A. Di Mauro, M.E. Fragalà, V. Privitera, G. Impellizzeri, Mater. Sci. Semicond. Process. **69** (2017) 44.
- [6] S.H. Chaki, K.S. Mahato, T.J. Malek, M.P. Deshpande, J. Sci. Adv. Mater. Devices **2** (2017) 215.
- [7] L.M.P. Garcia, M.T.S. Tavares, N.F. Andrade Neto, R.M. Nascimento, C.A. Paskocimas, E. Longo, M.R.D. Bomio, F.V. Motta, J. Mater. Sci. Mater. Electron. **29** (2018) 6530.
- [8] C. Nefzi, M. Souli, Y. Cuminal, N. Kamoun-Turki, Superlattices Microstruct. **124** (2018) 17.
- [9] C. Wang, T. Liu, X. Wang, J. Li, H. Jin, J. Yu, M. Yi, Y. Mo, Sens. Actuators B Chem. **270** (2018) 518.
- [10] J. Tian, Y. Sang, Z. Zhao, W. Zhou, D. Wang, X. Kang, H. Liu, J. Wang, S. Chen, H. Cai, H. Huang, Small **9** (2013) 3864.
- [11] H. Abdullah, M.R. Khan, M. Pudukudy, Z. Yaakob, N.A. Ismail, J. Rare Earths **33** (2015) 1155.
- [12] B. Li, B. Zhang, Q. Guan, S. Chen, P. Ning, Int. J. Hydrog. Energy **43** (2018) 19010.
- [13] L. Jing, J. Zhou, J.R. Durrant, J. Tang, D. Liu, H. Fu, Energy Environ. Sci. **5** (2012) 6552.
- [14] C. Han, L. Yan, W. Zhao, Z. Liu, Int. J. Hydrog. Energy **42** (2017) 12276.
- [15] J. Yi, H. Mo, B. Zhang, J. Song, D. Liu, G. Zhuo, Sep. Purif. Technol. **211** (2019) 474.
- [16] J.C. Cano-Franco, M. Álvarez-Láinez, Mater. Sci. Semicond. Process. **90** (2019) 190.
- [17] C.A. Schneider, W.S. Rasband, K.W. Eliceiri, Nat. Methods **9** (2012) 671.
- [18] N.F. Andrade Neto, Y.G. Oliveira, C.A. Paskocimas, M.R.D. Bomio, F.V. Motta, J. Mater. Sci. Mater. Electron. **29** (2018) 19052.
- [19] D.L. Wood, J. Tauc, Phys. Rev. B **5** (1972) 3144.
- [20] V.Y. Zenou, S. Bakardjieva, Mater. Charact. **144** (2018) 287.
- [21] D. Portnikov, H. Kalman, Powder Technol. **336** (2018) 393.
- [22] M. Emami, R. Goodarzi, Optik **171** (2018) 397.
- [23] J. Singh, S.A. Khan, J. Shah, R.K. Kotnala, S. Mohapatra, Appl. Surf. Sci. **422** (2017) 953.
- [24] P. Kumar, B. Ahmad, F. Chand, K. Asokan, Appl. Surf. Sci. **452** (2018) 217.
- [25] F.V. Motta, A.P.A. Marques, J.W.M. Espinosa, P.S. Pizani, E. Longo, J.A. Varela, Curr. Appl. Phys. **10** (2010) 16.
- [26] E. Nurfani, M.A.K. Purbayanto, T. Aono, K. Takase, Y. Darma, Opt. Mater. **84** (2018) 453.
- [27] S. Rehman, A. Mumtaz, S.K. Hasanain, J. Nanoparticle Res. **13** (2011) 2497.
- [28] E. Şilik, S. Pat, S. Özen, R. Mohammadigharehbagh, H.H. Yudar, C. Musaoğlu, Ş. Korkmaz, Thin Solid Films **640** (2017) 27.
- [29] M. Kang, S.W. Kim, H.Y. Park, J. Phys. Chem. Solids **123** (2018) 266.
- [30] Y. Li, W. Song, J. Liu, Z. Zhao, M. Gao, Y. Wei, Q. Wang, J. Deng, Chem. Eng. J. **330** (2017) 926.
- [31] C. Liu, H. Tai, P. Zhang, Z. Yuan, X. Du, G. Xie, Y. Jiang, Sens. Actuators B Chem. **261** (2018) 587.
- [32] M.M. Momeni, M. Hakimian, A. Kazempour, Ceram. Int. **41** (2015) 13692.
- [33] V. Madhavi, P. Kondaiah, G. Mohan Rao, Appl. Surf. Sci. **436** (2018) 708.
- [34] F. Bensouici, M. Bououdina, A.A. Dakhel, R. Tala-Ighil, M. Tounane, A. Iratni, T. Souier, S. Liu, W. Cai, Appl. Surf. Sci. **395** (2017) 110.
- [35] P. Singh, K.M.K. Srivatsa, A. Barvat, P. Pal, Curr. Appl. Phys. **16** (2016) 1388.
- [36] G.H. Tariq, D.W. Lane, M. Anis-ur-Rehman, Appl. Phys. A **120** (2015) 1407.
- [37] Y. Tan, S. Zhang, R. Shi, W. Wang, K. Liang, Int. J. Hydrog. Energy **41** (2016) 5437.
- [38] S.-M. Oh, S.-S. Kim, J.E. Lee, T. Ishigaki, D.-W. Park, Thin Solid Films **435** (2003) 252.
- [39] K. Dai, Z. Chen, L. Lu, G. Zhu, Z. Liu, Q. Liu, Thin Solid Films **539** (2013) 23.
- (Rec. 11/04/2019, Rev. 17/07/2019, 26/11/2019, Ac. 30/11/2019)